FRACTURE ENERGY AND STRENGTH BEHAVIOR OF A SODIUM-BOROSILICATE GLASS-Al_2O_3 COMPOSITE SYSTEM

F. F. Lange
Material Sciences Department

Technical Report No. 6
N00014-68-C-0323

April 1, 1971

WESTINGHOUSE RESEARCH LABORATORIES
Beulah Road, Churchill Boro
Pittsburgh, Pennsylvania 15235

FRACTURE ENERGY AND STRENGTH BEHAVIOR OF A SODIUM-BOROSILICATE GLASS-Al_2O_3 COMPOSITE SYSTEM

F. F. Lange
Material Sciences Department

Technical Report No. 6
N00014-68-C-0323

April 1, 1971

WESTINGHOUSE RESEARCH LABORATORIES
Beulah Road, Churchill Boro
Pittsburgh, Pennsylvania 15235

FOREWORD

This report was prepared at the Westinghouse Research and Development Center, Pittsburgh, Pennsylvania 15235. The work was sponsored by the Office of Naval Research under Contract Number N00014-68-C-0323.

ABSTRACT

Both the fracture energy and strength have been determined for a sodium-borosilicate glass-Al_2O_3 dispersed composite system. Three composite series within this system were investigated. Each series contained a different average particle size Al_2O_3 dispersion, viz. $\overline{3.5}$, $\overline{11}$, and $\overline{44}$ μm. Within each series, composites were vacuum hot-pressed that contained .10, .25 and .40 volume fractions of the Al_2O_3 dispersed phase. The fracture energy was determined at 77°K with the double cantilever specimen configuration. Strength measurements were carried out using a four-point flexural test.

A significant increase in fracture energy was observed (up to 5 times the fracture energy of the glass without a second phase dispersion). The fracture energy depended on both the interparticle spacing and average particle size of the Al_2O_3 dispersion. These results could best be explained by a previously proposed model for the interaction of a crack front with a second phase dispersion. Surface roughness also contributed to the increased fraction energy.

Some composites exhibited a significant strengthening relative to the glass without a dispersion. Calculated values of the crack size showed that the Al_2O_3 dispersion increased the crack size of the glass by an amount equal to $\sim$ 1-3 times the average

particle size of the Al_2O_3 dispersion. Thus, the Al_2O_3 dispersion increased both the fracture energy and the crack size. These two opposing parameters ultimately determined the strength behavior of these composites.

INTRODUCTION

Recently it has been suggested[1] that the fracture energy of a brittle material should depend, in part, on the spacing between inhomogeneities within the brittle material. Briefly stated, this suggestion is based on observations that a crack front increases its length when it interacts with a second phase dispersion (e.g., voids, precipitated particles, etc.) within a brittle matrix. Using the concept that the crack front possesses a line energy, such an increase in crack front length should require energy, thus increasing the energy required to initiate crack propagation. Because fracture energy is one of the three factors that control the strength of materials,[2] an increase in fracture energy might be expected to increase a material's strength.

Extensive strength data reported by Hasselman and Fulrath[3] indicated that the strength of a certain glass-Al_2O_3 composite system depended on the spacing between the Al_2O_3 dispersed particles. Since these data were in good agreement with the functional relation predicted by the interaction of a crack front with a dispersed, second phase, the fracture energy of this composite system was investigated. The results of this investigation will be reported here.

MATERIAL PREPARATION

The glass (70 wt% SiO_2, 16 wt% Na_2O, 14 wt% B_2O_3) was prepared in a similar manner as described by Hasselman and Fulrath.[3] To avoid excessive water and gas absorption during melting, which appeared to affect the hot-pressing behavior of the glass powder, the constituent powders (SiO_2, Na_2CO_3 and H_2BO_3) were calcined at 700°C for 4 hrs before the temperature was raised to 1350°C to form a fluid medium. After two hours at this temperature, a glass was formed by pouring the fluid mass onto a stainless steel plate. Glass powder (average particle size < 5 μm) was prepared by crushing and dry milling. The density of this glass was measured as 2.477 $\pm$ .002 g/cm^3 by both an Archimedes technique on the bulk glass and a pycnometer technique on the milled powder. The thermal expansion of this glass was measured as 8×10^{-6}/°C (25°C-400°C), which is approximately equal to the average thermal expansion of Al_2O_3.[4]

Composite powders were formed by mixing the proper volume fractions of the chosen average particle size Al_2O_3 powder in acetone with a dispersing agent (DuPont 'Merpol' HC). Mixing was carried out for 16 hrs within a rotating plastic bottle in which several Al_2O_3 balls were used to break up aggromerates. The small amount of plastic picked up during mixing was burned off at 400°C. The densities of

these composite powders (measured using a pycnometer) agreed with calculations based on volume fraction considerations.

Three different average particle size Al_2O_3 powders were used*, viz. a $\overline{3.5}$ μm powder, a $\overline{11}$ μm powder, and a $\overline{44}$ μm powder. Both the $\overline{3.5}$ μm and $\overline{11}$ μm powders had an angular morphology. The $\overline{44}$ μm powder consisted of polycrystalline spheres. The average particle size was determined by taking micrographs of powder samples and measuring the particle size directly. The spread of the particle size was approximately $\pm$ 50% of the average size for all powders.

Discs of the different glass-Al_2O_3 composites were vacuum hot-pressed using a similar technique described by Hasselman and Fulrath.[3] In the initial stages of this investigation, it was found that during hot-pressing, gases were continuously emitted from the glass powder. This was confirmed by a moisture analysis carried out between 25°C-800°C. The continuous emission of water vapor and presumably other gases, resulted in residual porosity during the initial hot-pressing attempts. Reduction of this porosity was accomplished by slowly increasing the temperature ($\sim$ 1°C/min) during the last portion of the hot-pressing schedule (between 600°C-700°C), to keep the vacuum in the 10^{-5} torr range. After hot pressing, the composite discs were annealed at 600°C for 2 hrs to relieve any residual stresses.

---

* $\overline{3.5}$ μm: ALCOA Corporation

$\overline{11}$ μm: Muller Corporation

$\overline{44}$ μm: Zircoa Corporation

Annealing was found necessary to diamond cut the fracture energy specimens. Table I lists the hot-pressed glass and glass-composites with their measured porosity as determined by the Archimedes technique.

FRACTURE ENERGY DETERMINATIONS

Fracture energy is a material property that indicates the amount of energy absorbed by a unit area of fractured surface at the moment of crack propagation. Many different specimen configurations are acceptable for determing fracture energy. Regardless of the specific configuration, the fracture energy is determined by measuring the force required to repropagate a sharp crack that had been previously introduced into a specimen. Knowing this force (F), the elastic modulus (E) of the material, the length (L) of the pre-existing crack and the specimen dimensions, the fracture energy can be calculated using a standard equation derived for the particular specimen configuration.

For ceramic materials, the double-beam cantilever specimen configuration has been widely used primarily because of the many techniques that have been developed to introduce a sharp crack into this configuration. Figure 1 shows this specimen configuration and the approximate specimen dimensions used to determine the fracture energy of the glass-Al_2O_3 composite materials. The equation used to calculate the fracture energy (γ) for this configuration was derived by both Gross and Srawley[5] and Wiederhorn et al.[6] Equation (1) illustrates Wiederhorn's solution:

$$\gamma = [6\ F^2L^2/E\ w^2t^3][1 + 1.32\ t/L + 0.542\ (t/L)^2]. \qquad (1)$$

He found that this equation was valid when the ratio of the crack length (L) to the beam width (t) was greater than 1.5.

Specimens were prepared by diamond cutting rectangular plates from the hot-pressed glass-Al_2O_3 discs. Holes for load application were introduced with an ultrasonic impact grinder. Both sides of each specimen were polished to allow an optical measurement of the crack length prior to fracture. Sharp cracks were introduced by first slotting each specimen with a 6 mil diamond blade and then wedging the slot open under a microscope to introduce a small sharp crack from the end of the slot. The crack length was measured with a microscope-cathetometer. The ratio of the crack length to specimen width was kept between 1.6-2.1.

The specimens were then annealed at 400°C for 2 hrs. Preliminary experiments showed that annealing did not change the crack length but it did reduce the data scatter.

All fracture energy determinations were conducted in an ambient of liquid nitrogen to reduce the influence of stress-corrosion during loading.[7] The apparatus used for loading was duplicated from that used by Wiederhorn. The loading was carried out by an Instron with a fixed cross head speed of 0.05 cm/min.

The room temperature elastic properties for this glass-Al_2O_3 composite system has been previously reported by Hasselman and Fulrath.[8]

These elastic data were required to calculate the fracture energy (see Eq. (1)). Since the fracture energy determinations were carried out at 77°K, it was necessary to determine whether or not the room temperature elastic property data could be used at 77°K. To do this, the elastic modulus of the hot-pressed glass (without the dispersed, second phase) was determined at 77°K by a sonic pulse technique. This low temperature data agreed to within $\pm$ 2% of the room temperature data reported by Hasselman and Fulrath. With this confirmation and with the knowledge that the elastic properties of Al_2O_3 only change 1.7% between 77-300°K,[9] the reported room temperature elastic properties were used to calculate the fracture energy at 77°K. It was also assumed that the elastic modulus of those specimens that contain some residual porosity was the same as a fully dense composite.

After the fracture energy determinations were made, representative fracture surfaces were observed using both scanning electron microscopy and optical microscopy.

Many preliminary experiments were conducted to determine the precision and reproducibility of this technique to determine fracture energy. One of these experiments was to determine the fracture energy of a glass* that Wiederhorn[10] had previously reported. The agreement between these two determinations was excellent: Wiederhorn's value: $4.52 \pm 4.2\% \times 10^3$ ergs/cm^2, author's value:** $4.48 \pm 5\% \times 10^3$ ergs/cm^2.

---

* Composition: .72 SiO_2, .02 Al_2O_3, .14 Na_2O, .01 K_2O, .04 MgO, .07 CaO.

** Specimen size was the same shown in Fig. 1. This value represents the average of six specimens.

STRENGTH MEASUREMENTS

Four point flexural strength measurements were made at room temperature on specimens that were diamond cut to .07 x .20 x 1.5 cm from the fractured, double cantilever specimens. Six specimens were tested for each glass-Al_2O_3 composite. The cross-head rate was .05 cm/min.

Strength measurements were carried out for two reasons. First, it was of interest to determine the relation between fracture energy, strength and microstructure. Second, it was of interest to compare the strength of these specimens to those reported by Hasselman and Fulrath.[3]

RESULTS

The fracture energies of the glass-Al_2O_3 composite specimens are given in Table I. Each value represents the average of 6-10 specimens. Figure 2 illustrates the fracture energy, volume fraction relation in graphical form. Two important results were obtained from these data:

1. The fracture energy of the glass can be significantly increased by incorporating a Al_2O_3 second-phase dispersion.
2. The fracture energy for this composite system depends on both the volume fraction and the average particle size of the Al_2O_3 dispersed, second phase.

Strengths of these composites are illustrated in Fig. 3. These data are also given in Table I. The strength of the glass without a dispersed phase (13,600 $\pm$ 11% psi) was similar to that reported by Hasselman and Fulrath[3] (14,700 $\pm$ 12.7% psi). The significant strengthening will be discussed in the next section as related to the fracture energy, the elastic modulus and the composite microstructure.

Representative fracture surfaces are shown in Fig. 4 for the .10 volume fraction $\overline{3.5}$ μm, $\overline{11}$ μm, and $\overline{44}$ μm average particle size composites. Although the surface roughness appeared similar for all

composites, there was a difference in topography associated with the particles for both low and high volume fraction composites. For low volume fractions of the dispersed Al_2O_3 phase (such as that shown in Fig. 4), individual particles could be easily identified on the fractured surface. Steps associated with most of the particles, indicating the interaction of the crack front with the particles,[1] could clearly be seen for these composites. As the volume fraction increased, the interparticle spacing decreased and the steps associated with the particle became less distinquishable. This was particularly pronounced for the $\overline{3.5}$ μm composite series. The fracture surface of the $\overline{3.5}$ μm, .40 volume composite appeared similar to that of a polycrystalline material.

For both the $\overline{3.5}$ μm and $\overline{11}$ μm composites, the crack propagated around most of the dispersed particles and not through them. For the $\overline{44}$ μm composites, the crack front traversed most of the large spherical polycrystalline particles.

DISCUSSION

Fracture Energy of the Glass-Composite System

Four possible mechanisms might be responsible for the fracture energy behavior reported above:

1. Equation (1) assumes a smooth fracture surface. Thus an increase in fracture surface area due to surface roughness will increase the calculated value of the fracture energy.
2. Energy might be absorbed by the second phase dispersion, e.g., by plastic deformation.
3. Friction between parting fracture surfaces can absorb energy during fracture.
4. Interaction of the crack front with the second phase dispersion has been suggested as a mechanism for increasing the fracture energy.[1]

The contribution of each of these energy absorbing mechanisms will be discussed.

The composite fracture surfaces were observed to be rough relative to the smooth fracture surfaces of the glass without the second-phase dispersion. The fractional increase in surface area can be estimated by assuming a periodic geometry for the surface roughness.

Such an estimate has been made assuming a plane surface containing cubic protrusions representing the protruding second-phase particles within the glass matrix. Two results were obtained from this analysis:

1. The fractional surface area increase per unit of apparent area only depends on the volume fraction of the second-phase dispersion - regardless of particle size.

2. A relatively small increase in fractional surface area is obtained, e.g., the fractional increase is 0.1 for 0.10 volume fraction of second phase dispersion, increasing to 1.5 for 0.50 volume fraction.

Thus, the rough surface topography of the composite specimens should only contribute a portion (a factor < 2) to the observed increase in fracture energy. Also, this mechanism could not be responsible for the observed particle size dependence.

Energy absorption by the Al_2O_3 dispersed phase should be negligible for several reasons. First, for both the $\overline{3.5}$ μm and the $\overline{11}$ μm composites, only a small fraction of the Al_2O_3 particles exhibited transparticle fracture. Second, the fracture energy for single crystal Al_2O_3 is approximately the same as that of the glass matrix;[11] thus, the fracture surfaces of those particles that did exhibit transgranular fracture should not require more energy to form than that for the glass matrix. The transparticle fracture of the polycrystalline spheres in the $\overline{44}$ μm composites can be examined in a similar manner. The fracture

energy of 10 μm polycrystalline Al_2O_3 is 1.61×10^4 ergs/cm^2 as measured by Swanson and Gross.[12] This value is much less than the values obtained for both the .25 and .40 volume fraction, $\overline{44}$ μm composites. Also, from fractional surface area considerations, the contribution of the fractured Al_2O_3 spheres would be small relative to the observed fracture energy of this composite series.

Although energy absorption by frictional forces has been shown not to occur for the formation of certain topographical fracture features, e.g., fracture steps,[13] this mechanism cannot be excluded for fiberous composite materials such as wood.[14] For the case of fiberous composites, it is conceivable that the plucking of loosely bonded fibers from the matrix material can result in surface friction. The two principle topographical features observed on the glass-Al_2O_3 composite fracture surfaces were fracture steps associated with the dispersed particles and surface roughness due to the crack path either avoiding or traversing the dispersed particles. These topographical features can be explained as being formed by the opening (tensile) mode of crack propagation. It was unlikely that fractional forces significantly contributed to the fracture energy in this composite system.

Pinning of a crack front at positions of second phase inhomogeneities within a brittle matrix has been observed by many investigators.[15,16] The author has recently reported[1] that the crack front bows out between each pair of pinning positions, thus increasing its total length prior to breaking away from these pinning positions.

It was shown that the fractional increase in the crack front length per unit crack extension depends on both the distance between the pinning positions and the curvature of the crack front between the pinning positions. Since the crack front possesses a line energy,[1,17] energy must be supplied to increase the length of the crack front. At the same time, energy must also be supplied to create the new fracture surfaces as the crack front moves between the pinning positions. Formalization of this model of crack propagation has resulted in the following expression for the fracture energy, i.e., the energy per unit area required to initiate fracture:

$$\gamma = \gamma_o + \frac{T}{d} . \qquad (2)$$

γ_o is the energy per unit area required to form new fracture surface; T is the critical* line energy per unit length of the crack front and d is the distance between pinning positions. In deriving this expression, the pinning positions were assumed to be points without dimensions and the crack front was assumed to bow out to form a semicircle between the pinning positions. An estimate for the critical line energy was also previously derived[1]

* The line energy depends on the applied stress. The critical stress required to propagate the crack defines the critical value of the line energy.[1]

$$T \simeq C \gamma_o \qquad (3)$$

where the value of C can be approximated by the crack size in the material. Substituting into this expression reasonable values of both C and γ_o for glass, e.g., C = .005 to .01 cm and γ = 3,000 to 6,000 ergs/cm^2, the line energy (T) of a crack front in a glass can be extimated to be between 15-60 ergs/cm.

The fracture energy data obtained during this investigation has been plotted as a function of the inverse average interparticle distance ($\frac{1}{d}$).* These plots are illustrated in Fig. 5. For each of the three composite series, a linear plot has resulted (the only datum point that does not lie on a linear plot is that one which represents the 0.40 VF, $\overline{3.5}$ μm composite). The slope of each linear plot, which equals the line energy of the crack front, is given in Table II. The intercept is also given in this table.

When the fracture energy data is analyzed in this manner, three points stand out:

1. For each of the three series, the linear relation between fracture energy and $\frac{1}{d}$ is consistent with the proposed model for the

*From Fullman's equations[18] it can be shown that $d = 2D \frac{(1-VF)}{3\ VF}$, where D = average particle size and VF = volume fraction of the dispersed phase.

interaction of a crack front with a second phase dispersion (see Eq. (2)).

2. With the exception of the $\overline{3.5}$ μm series, the line energy values are close to the theoretical range predicted from Eq. (3).

3. The intercepts, representing the constant term in Eq. (2) are approximately 1.5-2.0 times the fracture energy of the glass without the second-phase dispersion.

Equation (2) predicts that the intercepts should be equal to the fracture energy of the glass, i.e., $\sim$ 6,000 ergs/cm^2. This equation did not take into account energy to create fracture surface due to surface roughness. As discussed above, a factor less than two is not unreasonable for the increase in fracture energy due to surface roughness. This could explain the intercept values obtained in Fig. 5.

The line energy of a crack front at the moment of crack propagation represents the volume intregal of the strain energy adjacent to the crack front just prior to the moment that atomic bonds are broken. Thus, from theoretical considerations, the line energy should be constant for any particular material. The line energy values for the three composite series appear to be in direct disagreement with this statement, i.e., a different line energy results for each composite series. Figure 6 illustrates the apparent line energy as a function of the average particle size of the Al_2O_3 dispersion. Since the proposed model does not predict this dependence, either the

model requires a change or the above statement concerning uniqueness of the line energy is incorrect. The author has chosen to change the model.

It is not inconceivable that the amount of bowing of the crack front between pinning positions depends on how well the pinning positions hold the crack front as it bows between them. This is illustrated in Fig. 7 by two sets of pinning positions. The distance between the pinning positions is the same for both sets, but their size in one set is much larger than in the other. The hypothesis is that the overlapping of the stress fields of the two different segments of the crack front in front of the pinning positions governs the breakaway position. For the smaller set shown in Fig. 7, the stress fields overlap each other for only a small amount of bowing because of the small size of the pinning positions. For the larger set, a greater amount of bowing takes place before the stress fields in front of the pinning position are sufficiently large to cause the crack front to breakaway. Thus, the larger the pinning position, the more effective it is in both pinning the crack front and allowing the crack front to increase its length before breaking away.

Incorporating this hypothesis into the model of crack propagation is straightforward. A dimensionless function F(D), dependent on the pinning size D, is incorporated into the second term of Eq. 2

$$\gamma = \gamma_o + F(D) \frac{T}{d} \qquad (4)$$

where $0 \leq F(D) \leq 1$. When the pinning positions have no effect on crack propagation, $F(D) = 0$ and the second term of the above equation has no effect on the fracture energy. As the size of the pinning positions increase and become more effective, F(L) increases its value and the second term becomes more significant.

The functional form of F(D), i.e., its dependence on pinning size D, can be determined directly from Fig. 6 for the case of the glass-Al_2O_3 composite system. F(D) is represented on the right hand ordinate of this figure, and it was arbitrarily chosen to have a value of 1.0 when T = 75 ergs/cm.

In summary, the fracture energy behavior exhibited by the glass-Al_2O_3 composite system is consistent with the concept that energy must be supplied to the crack front when it interacts with a second-phase dispersion. The following points support this agreement:

1. Fracture surface observations showed that the crack front bowed between the Al_2O_3 particles, resulting in the characteristic fracture steps associated with a pinned crack front.
2. Within each of the three composite series, the functional behavior of the fracture energy with respect to the interparticle distance was the same as that predicted by the model.

3. The observed dependence of the fracture energy on particle size is consistent with the hypothesis that smaller particles are not as effective in pinning a crack front as larger particles.

4. Interaction of the crack front with a second phase inhomogeneity also produces rough surfaces. Energy absorbed during fracture due to this surface roughness is approximately 1.5-2.0 times the fracture energy of the glass without a second phase dispersion. This is consistent with estimates made by others.[19]

Strength of the Glass-Al_2O_3 Composite System

The critical stress (σ_c) required to propagate a crack of length C depend on two material properties, viz. the elastic modulus (E) and the fracture energy (γ).[2] For a surface crack, this stress can be approximated by the following relation:[20]

$$\sigma_c = .89 \sqrt{\frac{2\gamma E}{\pi C}} . \qquad (5)$$

For the glass-Al_2O_3 composite system reported here, the strength, fracture energy*, and elastic modulii are known; thus the

* Fracture energy determinations were carried out at 77°K whereas strength measurements were obtained at room temp-rature. Wiederhorn has shown[10] that when stress-corrosion due to water vapor is minimized, the fracture energy values of glass is approximately the same at both temperatures. It has been assumed that this is also true for the glass-Al_2O_3 composite system.

crack size has been calculated for each composite. Table III summarizes these calculations. The significant results of these calculations are:

1. Within each of the three composite series, the crack size was approximately constant, i.e., the crack size was not significantly effected by the volume fraction of the Al_2O_3 dispersion.
2. The average crack size for the three composite series increased as the average particle size increased. This increase was much larger for the $\overline{44}$ μm series than for both the $\overline{3.5}$ μm and $\overline{11}$ μm series.

The first of these two results is in direct conflict with the strengthening model proposed by Hasselman and Fulrath[3] which they used to explain their strength data for seven glass-Al_2O_3 composites series of the same composition reported here. Their basic hypothesis was that the interparticle spacing controlled the crack size and thus the strength of their composites. It has been shown here that the particle size controls the crack size and that the interparticle spacing has little, if any, effect on crack size.

The second result shows that the crack size is related to the composite's microstructure, viz. the average crack size appears to depend, in part, on the particle size of the Al_2O_3 dispersion. The significant conclusion of this result is that the addition of a second phase dispersion will increase the crack size of the glass by an amount equal to approximately 1-3 times the average particle size of the dispersion.

Interpretation of the strength results in Fig. 3 can be made as follows. The three parameters that control strength, viz. fracture energy, elastic modulus and crack size, are known as a function of both the volume fraction and the average particle size of the Al_2O_3 dispersed phase:

1. The fracture energy increases as both the volume fraction and particle size of the Al_2O_3 dispersion increase (see Fig. 2). The functional relation is given by Eq. (2); i.e., $\gamma = \gamma_o + F(D) \frac{T}{d}$, where γ_o is equal to both the fracture energy of the glass without a dispersed phase and the increase due to surface roughness, i.e., $\gamma_o \cong$ 9000-12,000 ergs/cm^2, T = 75 ergs/cm and F(D) is given in Fig. 6.

2. The elastic modulus depends only on volume fraction.[21] Hasselman and Fulrath have reported the functional relation for this composite system.[8]

3. The crack size depends on the average particle size of the second phase dispersion. Assuming a surface crack configuration, this dependence can be approximated by: $C = C_o + 2D$, where $C_o = 29 \times 10^{-4}$ cm (the average crack size in the glass without a dispersed phase).

These relations where substituted into Eq. (5) to calculate the strength of each composite within the seven composite series, viz. $\overline{15}$, $\overline{21}$, $\overline{25}$, $\overline{32}$, $\overline{42}$, $\overline{51}$, $\overline{60}$ μm that were prepared and investigated by Hasselman and Fulrath.[3] A value of F(D) = 1.0 was used for $D \geq 44$ μm

(see Fig. 6). The calculated strengths were compared with those measured by Hasselman and Fulrath. Figure 8 illustrates this comparison for both the smallest ($\overline{15}$ μm) and largest ($\overline{60}$ μm) average particle size series. In general, the agreement was good for those series where $D \leq \overline{32}$ μm. For $D \geq \overline{42}$ μm, the calculated strength values were smaller than the measured values for composites containing small volume fractions of the dispersed, second phase.

CONCLUSIONS

The fracture energy of a sodium-borosilicate glass could be significantly increased by incorporating a second-phase dispersion of Al_2O_3 particles. The fracture energy behavior was related to both the interparticle spacing and the average particle size of the Al_2O_3 dispersion. This behavior could best be explained by a previously proposed model which was based on the interaction of a crack front with a second-phase dispersion. Using the concept, the fracture energy data indicated that the larger particle size dispersions were more effective in interacting with the crack front than the smaller particle size dispersions. This was also one of the principle conclusions of similar study on an epoxy - $Al_2O_3.3H_2O$ composite system reported by Lange and Radford.[22]

A significant strengthening was measured for some of the composite materials. The average crack size of each composite (calculated from the strength, fracture energy, and elastic modulus) depended, in part, on the average particle size of the dispersed, second phase, viz. the calculated crack size increased from that of the glass without a dispersed phase by approximately 1-3 times the average particle size of the dispersed Al_2O_3 phase.

In general, if these concepts are to be applied to strengthen other brittle materials, a compromise must be made in the choice of the particle size of the dispersed phase. Although large particle size dispersions appear to result in a larger fracture energy than smaller particles, the larger particles also increase the size of the crack. Two other factors, viz. elastic modulus and residual stresses which have not been treated in this article, must also be considered when engineering the strength of brittle, particulate, composite material.

ACKNOWLEDGMENTS

The author thanks both J. R. Lynch and J. J. Nalevanko for the excellent technical service. Thanks also to S. M. Wiederhorn for helpful advice concerning fracture energy measurements and to K. C. Radford and R. J. Bratton for useful discussions. The work was sponsored by the Office of Naval Research, Contract No. N00014-68-C-0323.

REFERENCES

1. F. F. Lange, "The Interaction of a Crack Front with a Second-phase Dispersion," Phil. Mag., 22 [179], 983-92 (1970).
2. A. A. Griffith, "The Phenomena of Rupture and Flow in Solids," Phil. Trans. Roy. Soc. Lon., 221A [4], 163-198 (1920).
3. D. P. H. Hasselman and R. M. Fulrath, "Proposed Fracture Theory of a Dispersion-Strengthened Glass Matrix," J. Am. Ceram. Soc., 49 [2], 68-72 (1966).
4. J. B. Wachtman, Jr., T. G. Scuderi, and G. W. Cleek, "Linear Thermal Expansion of Al_2O_3 and ThO_2 from 100° to 1100°K," J. Am. Ceram. Soc., 45 [7], 319-23 (1961).
5. B. Gross and J. E. Srawley, "Stress-Intensity Factors by Boundary Collocation for Single-Edge-Notch Specimens Subject to Splitting Forces," NASA TN D-3295, February (1966).
6. S. M. Wiederhorn, A. M. Shorb and R. L. Moses, "Critical Analysis of the Theory of the Double Cantilever Method of Measuring Fracture-surface Energies," J. Appl. Phys., 39 [3], 1569-72 (1968).
7. S. M. Wiederhorn, "Fracture Surface Energy of Soda-Lime Glass," Materials Science Research Vol. 3, Ed. by W. W. Kriegel and H. Palmour III, Interscience, 503-28 (1966).

8. D. P. H. Hasselman and R. M. Fulrath, "Effect of Al_2O_3 Dispersions on Young's Modulus of a Glass," J. Am. Ceram. Soc., 48 [4], 218-19 (1965).

9. J. B. Wachtman, Jr., W. E. Tefft and D. G. Lan, Jr., "Young's Modulus of Single Crystal Corundum from 77 to 850°K," Mech. Prop. of Eng. Ceramics, Ed. by W. W. Kriegel and H. Palmour III, Inter-Science, 221-24 (1961).

10. S. M. Wiederhorn, "Fracture Surface Energy of Glass," J. Am. Ceram. Soc. 52 [2], 99-105 (1969).

11. S. M. Wiederhorn, "Fracture of Sapphire," J. Am. Ceram. Soc. 52 [9], 485-99 (1969).

12. G. D. Swanson and G. E. Gross, "Physical Parameters Affecting Fracture Strength and Fracture Mechanisms in Ceramics," Final Report, January 16, 1970, Contract No. N00019-69-C-0161, Naval Air Systems Command.

13. F. F. Lange and K. A. D. Lambe, "Interaction between a Crack Front and Cleavage Steps," Phil. Mag. 18 [151], 129-36 (1968).

14. H. G. Tattersal and G. Tappin, "The Work of Fracture and its Measurement in Metals, Ceramics and Other Materials," J. Mat. Sci. 1, 296-301 (1966).

15. H. Bethge, "Oberfachenstruckturen and Kristallbaufehler im elektronenmikroskopischen Bild, untersacht am NaCl(II)," Phys. Stat. Sol. 2, 775-820 (1962).

16. C. T. Forwood and A. J. Forty, "The Interaction of Cleavage Cracks with Inhomogeneities in NaCl Crystals," Phil. Mag. 11 [113], 1067-82 (1965).

17. J. Friedel, "Fracture," ed. by B. L. Averbach, D. K. Felbeck, G. T. Hahn and D. A. Thomas, John Wiley, 498 (1959).

18. R. L. Fullman, "Measurement of Particle Sizes in Opaque Bodies," Trans. AIME, J. Metals 197 [3], 447-52 (1953).

19. A. G. Evans and R. W. Davidge, "The Strength and Fracture of Stoichiometric Polycrystalline UO_2," J. Nuclear Materials 33, 249-60 (1969).

20. P. C. Paris and G. C. Sih, "Stress Analysis of Cracks," ASTM Spec. Tech. Pub. No. 381, 30-83 (1964).

21. Z. Hashin and S. Shtrikman, "A Variational Approach to the Theory of the Elastic Behavior of Multiphase Materials," J. Mech. Phys. Solids 11 [2], 127-40 (1963).

22. F. F. Lange and K. C. Radford, "Fracture Energy of an Epoxy Composite System," to be published by the Journal of Material Science.

FIGURE CAPTIONS

Fig. 1 The double-cantilever specimen configuration.

Fig. 2 Fracture energy of the three composite series vs volume fraction of the Al_2O_3 dispersed, second phase.

Fig. 3 Flexural strength of the three composite series vs the volume fraction of the Al_2O_3 dispersed, second phase.

Fig. 4 Fracture surfaces showing the surface topography associated with the .10 volume fraction composite; micrographs A, B, and C are from the $\overline{3.5}$ μm, $\overline{11}$ μm and $\overline{44}$ μm composite series, respectively. Fracture steps associated with the crack front interacting with the particles are illustrated with arrows.

Fig. 5 Fracture energy of the three composite series vs the average inverse interparticle spacing.

Fig. 6 Critical line energy (left-hand ordinate) vs the average particle size of the Al_2O_3 dispersed phase. The function F(D), representing the effectiveness of the pinning position, is plotted on the right-hand ordinate.

FIGURE CAPTIONS (continued)

Fig. 7 Illustration of the breakway position of a crack front from two different pairs of pinning positions, each separated by the same distance, d. The distance between the two arms of the crack front in front of each pinning position (illustrated by two arrows) is hypothesised to control the breakaway position due to the overlapping stress field. Large arrow is the direction of crack propagation.

Fig. 8 Comparison of strength data of two composite series reported by Hasselman and Fulrath[3] with strength values calculated from Eq. (5).

TABLE I

MECHANICAL PROPERTY DATA FOR THE SODIUM-BOROSILICATE GLASS-Al_2O_3 COMPOSITE SYSTEM

PARTICLE SIZE(μm)	VOLUME FRACTION	DENSITY, % THEORETICAL	ELASTIC* MODULUS (dyn/cm^2)	FRACTURE ENERGY ($ergs/cm^2$)	STRENGTH psi
GLASS	---	> 99	8.06×10^{11}	6280 ± 15%	13,600 ± 11%
	.10	> 99	9.25×10^{11}	10,600 ± 19%	15,800 ± 13%
$\overline{3.5}$	.25	97	11.4×10^{11}	12,700 ± 9%	19,500 ± 11%
	.40	93	14.4×10^{11}	12,800 ± 16%	24,300 ± 14%
	.10	> 99	9.25×10^{11}	10,400 ± 8%	15,500 ± 13%
$\overline{11}$	.25	99	11.4×10^{11}	13,800 ± 10%	21,900 ± 4%
	.40	97	14.4×10^{11}	19,800 ± 12%	26,200 ± 11%
	.10	> 99	9.25×10^{11}	15,600 ± 12%	10,200 ± 13%
$\overline{44}$	.25	98	11.4×10^{11}	22,700 ± 34%	12,500 ± 9%
	.40	95	14.4×10^{11}	29,900 ± 9%	20,800 ± 5%

* As reported by Hasselman and Fulrath[8]

TABLE II

THE CRITICAL LINE ENERGY VALUES AND INTERCEPT VALUES FOR THE THREE GLASS-Al_2O_3 COMPOSITE SYSTEMS

COMPOSITE SERIES: AVERAGE PARTICLE SIZE (μm)	CRITICAL LINE ENERGY (ergs/cm)	INTERCEPT (ergs/cm^2)
$\overline{3.5}$	2.3	9400
$\overline{11}$	12.0	8500
$\overline{44}$	75.0	12,000

TABLE III

CALCULATED CRACK SIZE VALUES FOR THE SODIUM-BOROSILICATE GLASS-Al_2O_3 COMPOSITE SYSTEM

COMPOSITE		CALCULATED CRACK SIZE (μm)	
AVERAGE PARTICLE SIZE (μm)	VOLUME FRACTION	INDIVIDUAL COMPOSITES	AVERAGE VALUE
GLASS	---	---	29
$\overline{3.5}$	.10	42	38
	.25	40	
	.40	33	
$\overline{11}$	.10	43	41
	.25	35	
	.40	45	
$\overline{44}$	.10	148	143
	.25	177	
	.40	106	

BLANK PAGE

Dwg. 2943A75

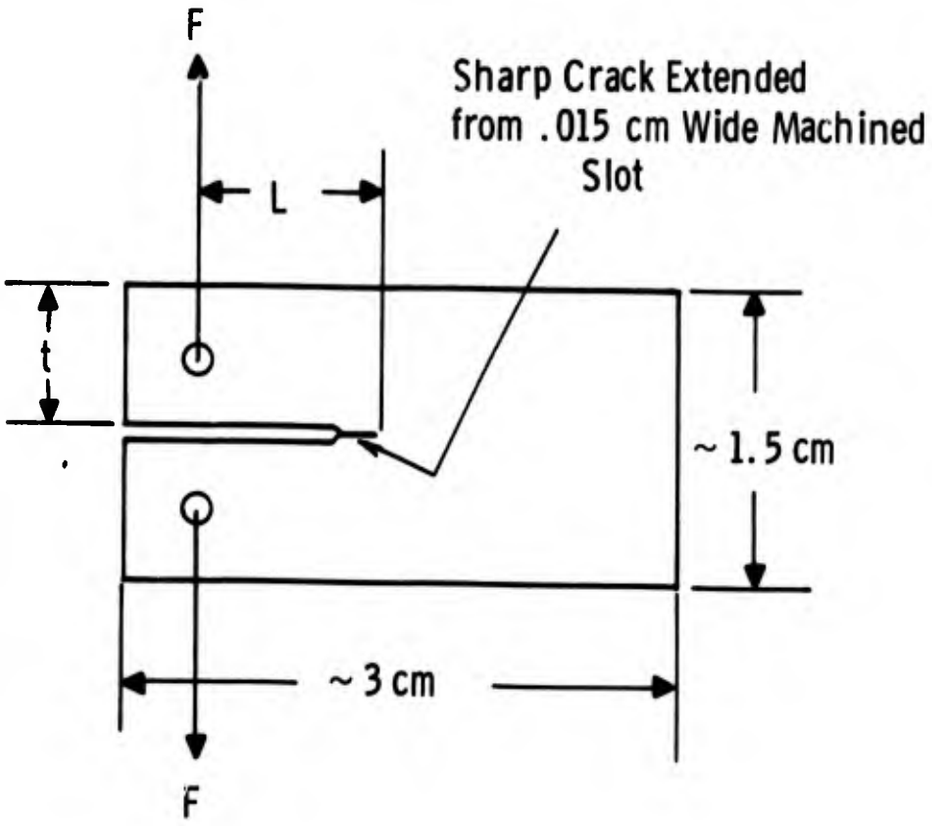

w = Thickness $\cong$ 0.07 cm

$$1.6 \leq \frac{L}{t} \leq 2.1$$

Fig. 1

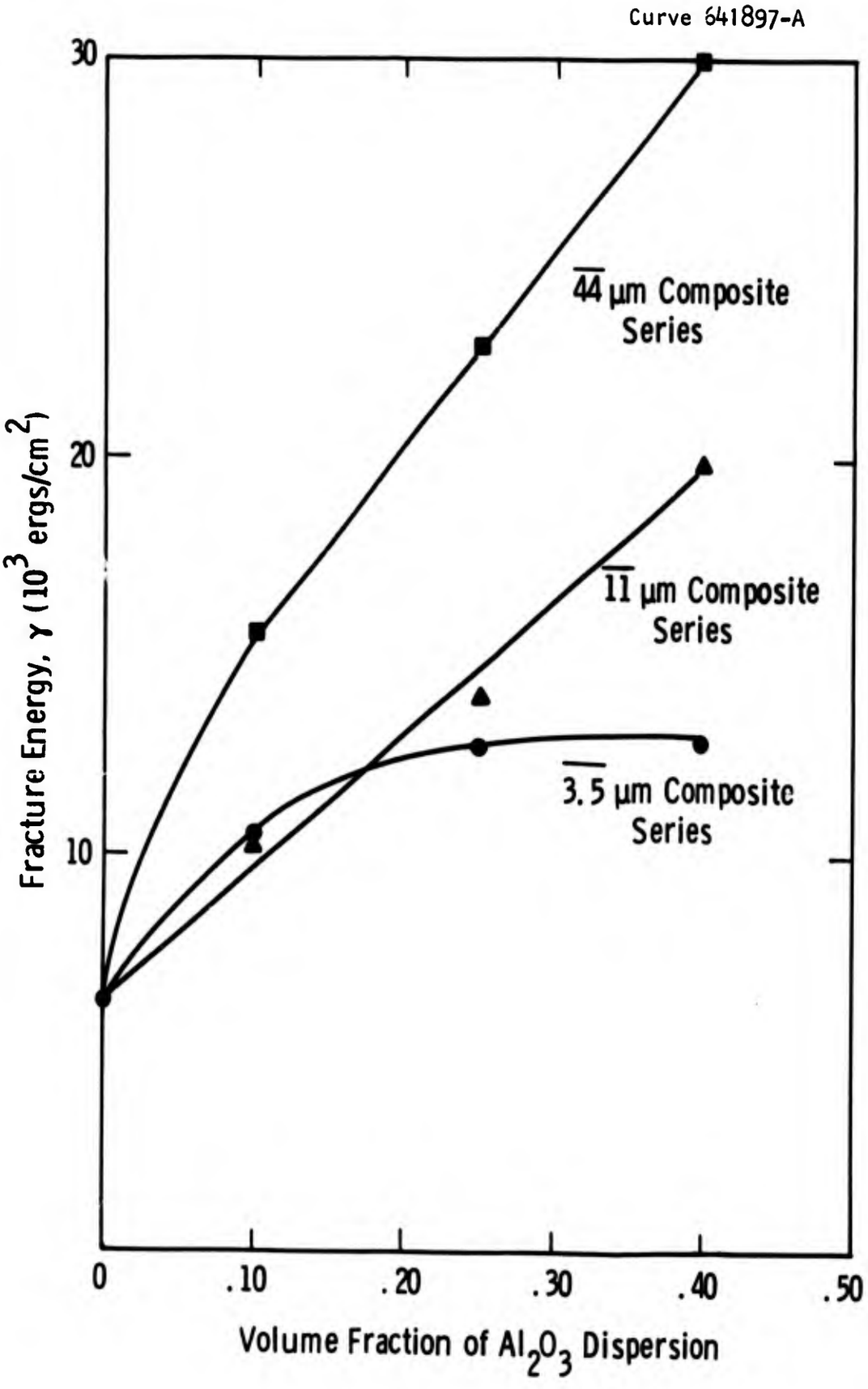
Curve 641897-A
30
20
10
0
.10
.20
.30
.40
.50
Fracture Energy, γ (10^3 ergs/cm^2)
Volume Fraction of Al2O3 Dispersion
44 μm Composite Series
11 μm Composite Series
3.5 μm Composite Series

Fig. 2

Curve 641898-A

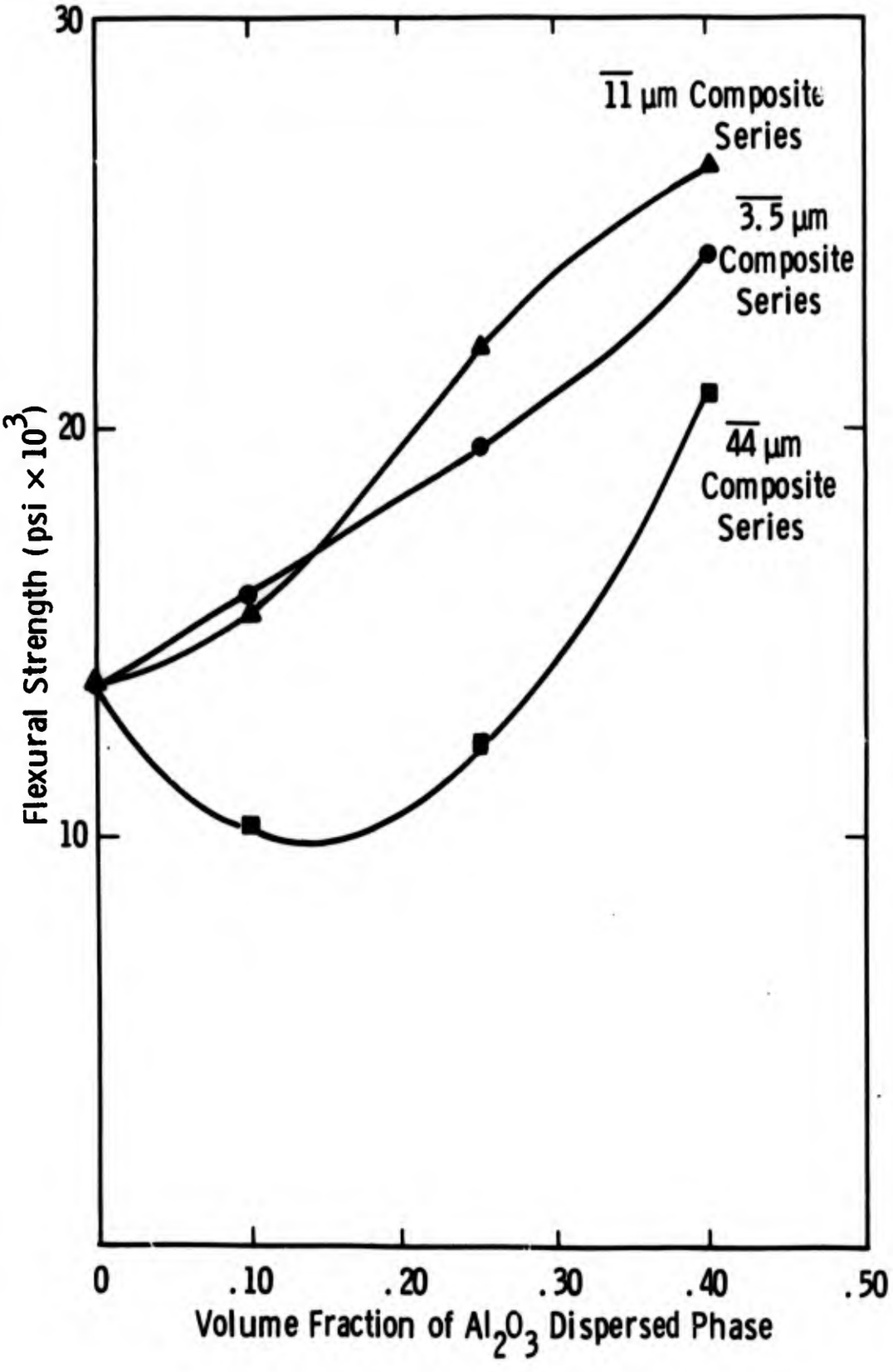

Fig. 3

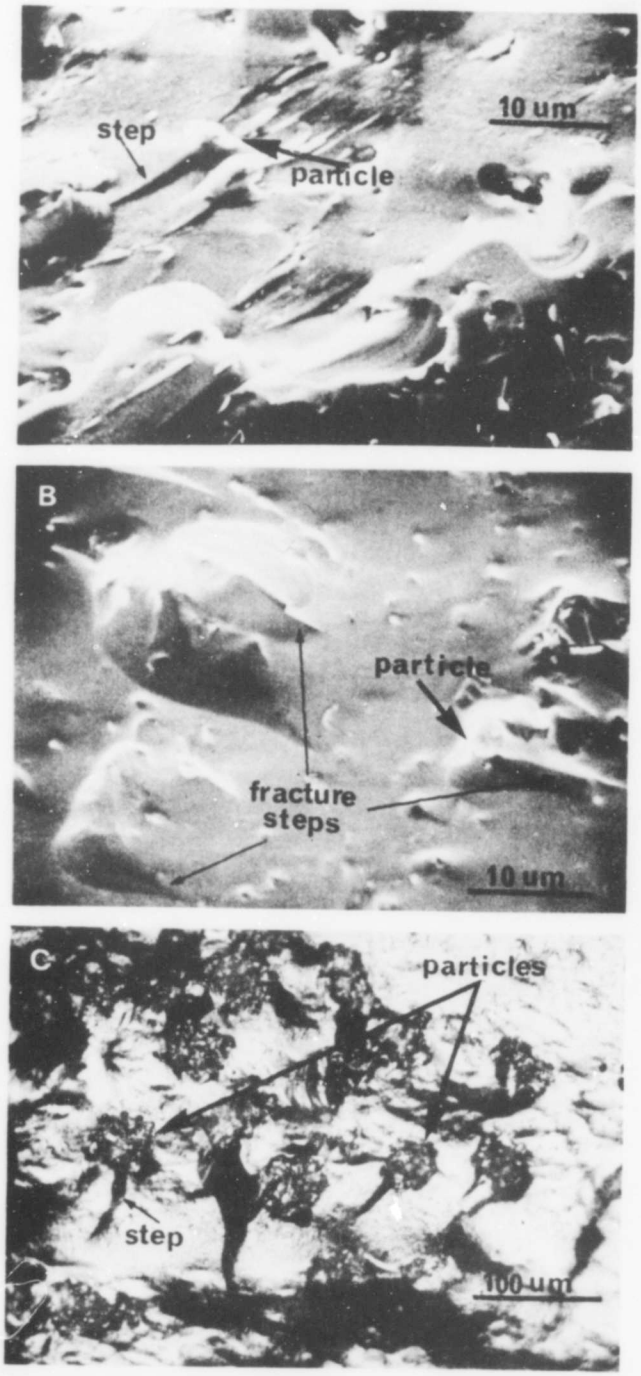
step
particle
10 um
B
particle
fracture
steps
10 um
C
particles
step
100 um

Fig. 4

Curve 641895-A

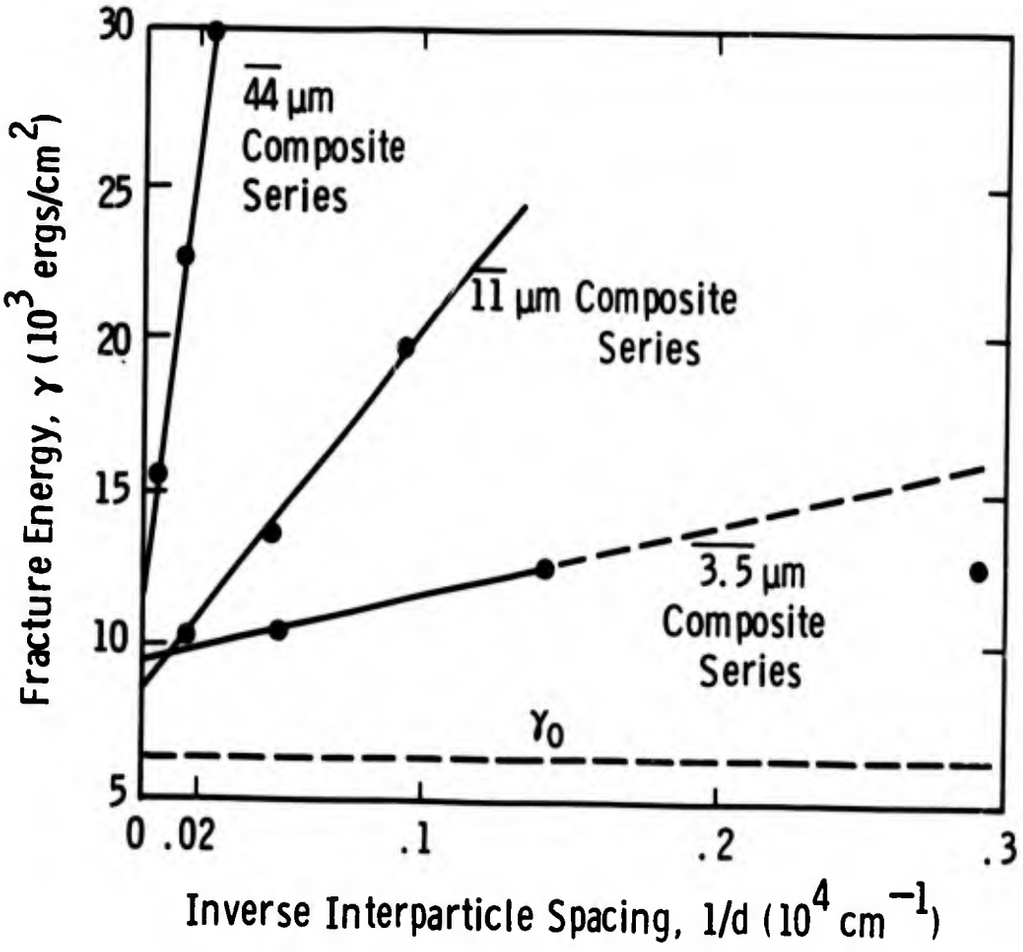

Fig. 5

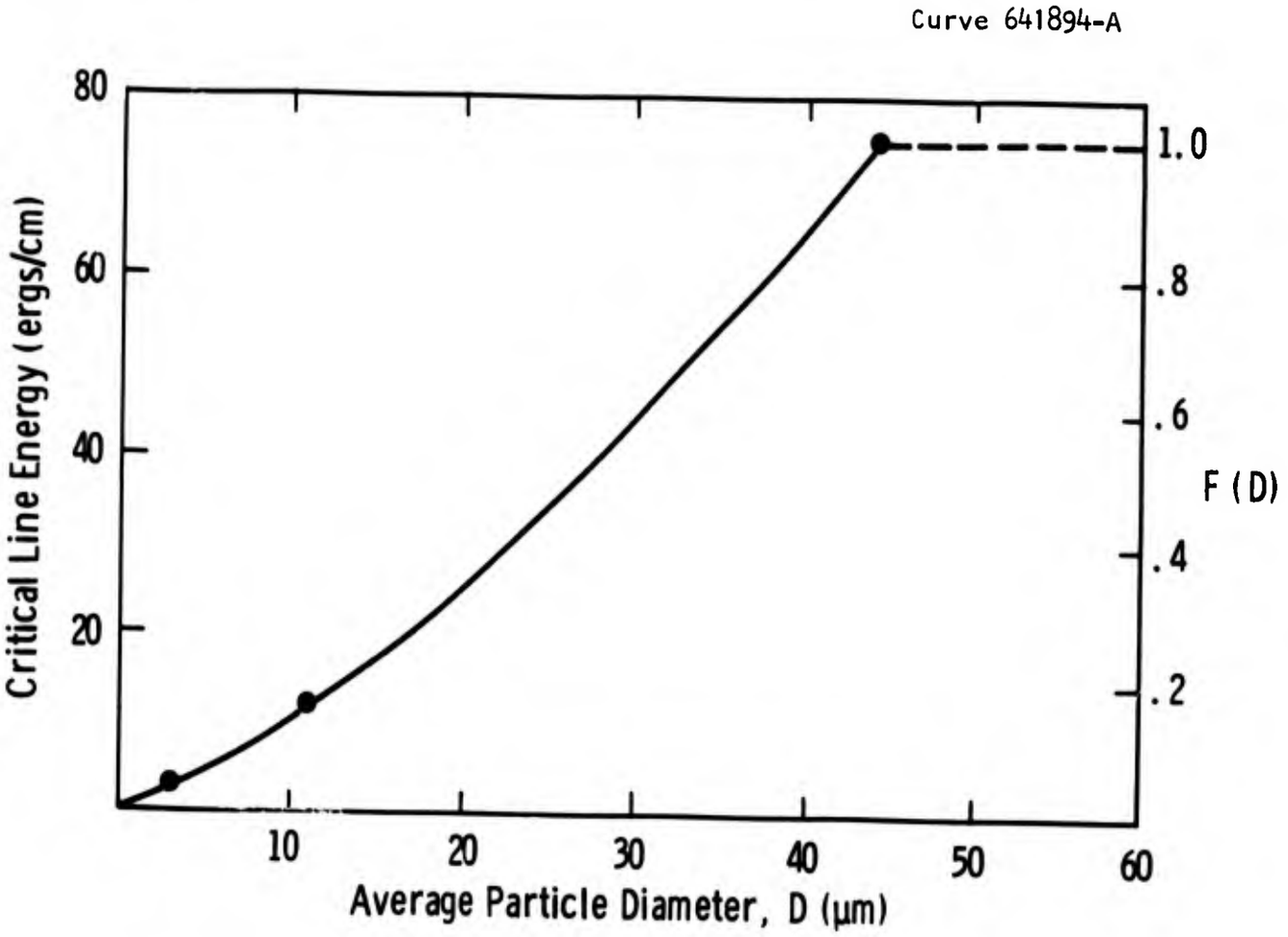
Curve 641894-A
Critical Line Energy (ergs/cm)
80
60
40
20
1.0
.8
.6
.4
.2
F (D)
10
20
30
40
50
60
Average Particle Diameter, D (μm)

Fig. 6

Dwg. 2943A74

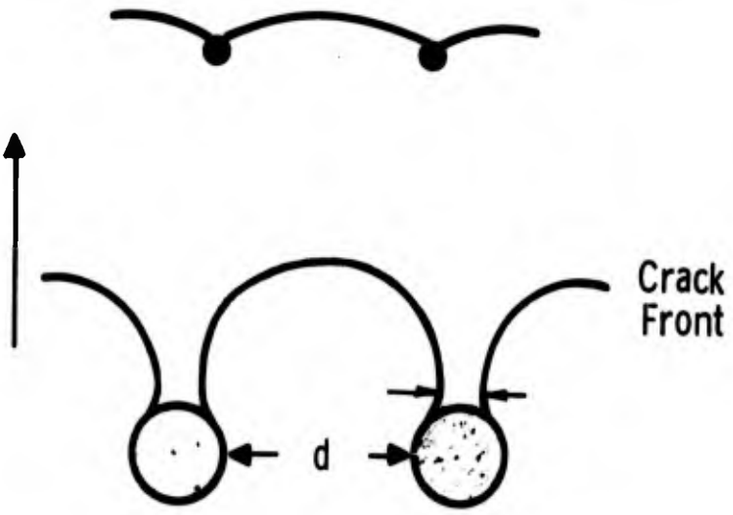

Fig. 7

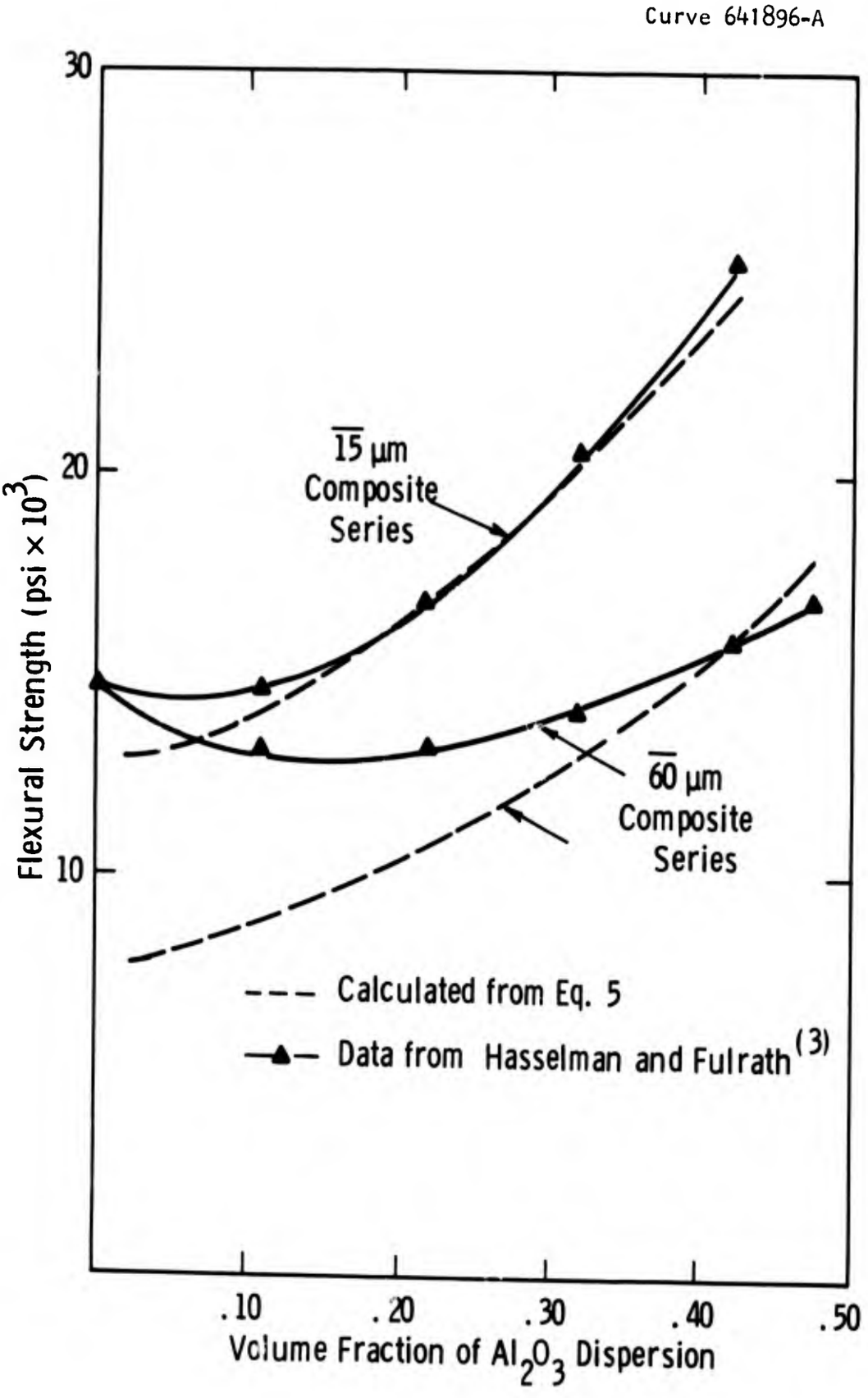
Curve 641896-A
30
20
10
Flexural Strength (psi × 10^3)
15 μm
Composite
Series
60 μm
Composite
Series
Calculated from Eq. 5
Data from Hasselman and Fulrath (3)
.10
.20
.30
.40
.50
Volume Fraction of Al2O3 Dispersion

Fig. 8

UNCLASSIFIED
Security Classification

DOCUMENT CONTROL DATA - R&D
(Security classification of title, body of abstract and indexing annotation must be entered when the overall report is classified)

1 ORIGINATING ACTIVITY (Corporate author) Westinghouse Electric Corporation Research Laboratories Pittsburgh, Pennsylvania 15235	2a REPORT SECURITY CLASSIFICATION UNCLASSIFIED 2b GROUP

3 REPORT TITLE

FRACTURE ENERGY AND STRENGTH BEHAVIOR OF A SODIUM-BOROSILICATE GLASS-Al_2O_3 COMPOSITE SYSTEM

4 DESCRIPTIVE NOTES (Type of report and inclusive dates)

Interim Technical Report

5 AUTHOR(S) (Last name, first name, initial)

F. F. Lange

6 REPORT DATE	7a TOTAL NO OF PAGES	7b NO OF REFS
April 1, 1971	45	22

8a CONTRACT OR GRANT NO.	9a ORIGINATOR'S REPORT NUMBER(S)
N00014-68-C-0323 b. PROJECT NO	71-9D2-CERAM-R1
c	9b OTHER REPORT NO(S) (Any other numbers that may be assigned this report)
d	NONE

10 AVAILABILITY/LIMITATION NOTICES

Reproduction in whole or in part is permitted for any purpose of the United States Government. Distribution of this document is UNLIMITED.

11 SUPPLEMENTARY NOTES	12 SPONSORING MILITARY ACTIVITY
	OFFICE OF NAVAL RESEARCH

13 ABSTRACT

A significant increase in fracture energy was observed (up to 5 times the fracture energy of the glass without a second phase dispersion). The fracture energy depended on both the interparticle spacing and average particle size of the Al_2O_3 dispersion. These results could best be explained by a previously proposed model for the interaction of a crack front with a second phase dispersion. Surface roughness also contributed to the increased fraction energy.

Some composites exhibited a significant strengthening relative to the glass without a dispersion. Calculated values of the crack size showed that the Al_2O_3 dispersion increased the crack size of the glass by an amount equal to $\sim$ 1-3 times the average particle size of the Al_2O_3 dispersion. Thus, the Al_2O_3 dispersion increased both the fracture energy and the crack size. These two opposing parameters ultimately determined the strength behavior of these composites.

DD FORM 1 JAN 64 1473

UNCLASSIFIED
Security Classification

RM 35054

14 KEY WORDS	LINK A		LINK B		LINK C	
	ROLE	WT	ROLE	WT	ROLE	WT
Ceramic composites						
Fracture energy						
Crack propagation						
Strength						

INSTRUCTIONS

1. ORIGINATING ACTIVITY: Enter the name and address of the contractor, subcontractor, grantee, Department of Defense activity or other organization *(corporate author)* issuing the report.

2a. REPORT SECURITY CLASSIFICATION: Enter the overall security classification of the report. Indicate whether "Restricted Data" is included. Marking is to be in accordance with appropriate security regulations.

2b. GROUP: Automatic downgrading is specified in DoD Directive 5200.10 and Armed Forces Industrial Manual. Enter the group number. Also, when applicable, show that optional markings have been used for Group 3 and Group 4 as authorized.

3. REPORT TITLE: Enter the complete report title in all capital letters. Titles in all cases should be unclassified. If a meaningful title cannot be selected without classification, show title classification in all capitals in parenthesis immediately following the title.

4. DESCRIPTIVE NOTES: If appropriate, enter the type of report, e.g., interim, progress, summary, annual, or final. Give the inclusive dates when a specific reporting period is covered.

5. AUTHOR(S): Enter the name(s) of author(s) as shown on or in the report. Enter last name, first name, middle initial. If military, show rank and branch of service. The name of the principal author is an absolute minimum requirement.

6. REPORT DATE: Enter the date of the report as day, month, year, or month, year. If more than one date appears on the report, use date of publication.

7a. TOTAL NUMBER OF PAGES: The total page count should follow normal pagination procedures, i.e., enter the number of pages containing information.

7b. NUMBER OF REFERENCES: Enter the total number of references cited in the report.

8a. CONTRACT OR GRANT NUMBER: If appropriate, enter the applicable number of the contract or grant under which the report was written.

8b, 8c, & 8d. PROJECT NUMBER: Enter the appropriate military department identification, such as project number, subproject number, system numbers, task number, etc.

9a. ORIGINATOR'S REPORT NUMBER(S): Enter the official report number by which the document will be identified and controlled by the originating activity. This number must be unique to this report.

9b. OTHER REPORT NUMBER(S): If the report has been assigned any other report numbers *(either by the originator or by the sponsor)*, also enter this number(s).

10. AVAILABILITY LIMITATION NOTICES: Enter any limitations on further dissemination of the report, other than those imposed by security classification, using standard statements such as:

(1) "Qualified requesters may obtain copies of this report from DDC."

(2) "Foreign announcement and dissemination of this report by DDC is not authorized."

(3) "U. S. Government agencies may obtain copies of this report directly from DDC. Other qualified DDC users shall request through

_____."

(4) "U. S. military agencies may obtain copies of this report directly from DDC. Other qualified users shall request through

_____."

(5) "All distribution of this report is controlled. Qualified DDC users shall request through

_____."

If the report has been furnished to the Office of Technical Services, Department of Commerce, for sale to the public, indicate this fact and enter the price, if known.

11. SUPPLEMENTARY NOTES: Use for additional explanatory notes.

12. SPONSORING MILITARY ACTIVITY: Enter the name of the departmental project office or laboratory sponsoring *(paying for)* the research and development. Include address.

13 ABSTRACT: Enter an abstract giving a brief and factual summary of the document indicative of the report, even though it may also appear elsewhere in the body of the technical report. If additional space is required, a continuation sheet shall be attached.

It is highly desirable that the abstract of classified reports be unclassified. Each paragraph of the abstract shall end with an indication of the military security classification of the information in the paragraph, represented as *(TS), (S), (C), or (U)*.

There is no limitation on the length of the abstract. However, the suggested length is from 150 to 225 words.

14. KEY WORDS: Key words are technically meaningful terms or short phrases that characterize a report and may be used as index entries for cataloging the report. Key words must be selected so that no security classification is required. Identifiers, such as equipment model designation, trade name, military project code name, geographic location, may be used as key words but will be followed by an indication of technical context. The assignment of links, rules, and weights is optional.